PERGAMON

International Journal of Solids and Structures 37 (2000) 3479–3501

INTERNATIONAL JOURNAL OF SOLIDS and STRUCTURES

www.elsevier.com/locate/ijsolstr

Failure of laminated composites at thickness discontinuities under complex loading and elevated temperatures

S. Lee, W.G. Knauss*

Graduate Aeronautical Laboratories, California Institute of Technology, Pasadena CA 91125, USA

Received 26 February 1998; in revised form 20 July 1998

Abstract

Failure initiation of laminated composites with discontinuous thickness has been studied in terms of typical structural load description (tension, shear force and bending moment) rather than in terms of micromechanics considerations. Four types of specimens of different stacking sequence were examined to determine failure initiation, analyzed subsequently via a finite element analysis (ABAQUS) and divided into two groups that evoke cross-ply failure, on the one hand, and delamination type failure on the other. For uni-directional fiber orientation in the tension direction and across the interface, failure occurs through cracking and delamination. While the initiation strength for this failure mode is significantly higher than for cross-ply configurations, the residual strength after initiation increases only marginally (10%) beyond the initiation point. For cases involving cross-plies on either side of the interface, failure initiation occurs by matrix cracking. In these cases the residual load bearing capability was 25 to 35% higher than the corresponding failure initiation loads. The data are analyzed in terms of the Tsai-Hill criterion and in terms of an energy release criterion that has been discretized in a manner consistent with a non-singular treatment of the step "discontinuity". Assuming that time dependent aspects of the failure process are not dominant, elevated temperatures did not change the general results of how bending and tension loads interact, provided one accounts for stresses induced thermally in the tests; however the magnitude at which the failures occur depends on the temperature, with increasing temperature leading to decreasing load tolerance. © 2000 Elsevier Science Ltd. All rights reserved.

Keywords: Composite; Failure initiation; Thickness discontinuity; Combined loading; Thermal stress

1. Introduction

A recurring problem in designing structures with fiber reinforced composite materials is the potential

* Tel: +1-626-395-4524; fax: +1-626-304-0175;.
E-mail address: wgk@caltech.edu (W.G. Knauss).

0020-7683/00/$ - see front matter © 2000 Elsevier Science Ltd. All rights reserved.
PII: S0020-7683(99)00021-9

failure at thickness variations in the lay-up associated with the induced stress concentrations. Such questions arise in connection with stress variations in the vicinity of geometric discontinuities in the ply drop-off problem as well as with attachments of stringers and other frame structures to the skin of aircraft, for example. With respect to the evolution of structural instabilities the post buckling strength of compound structures is of considerable importance for the fail safe evaluation of engineering designs. Thus, a knowledge of when and how the degradation and loss of such shell stiffening impacts global structural strength is mandatory for design purposes.

Within the framework of solid mechanics any failure emanating from "sharp" corners elicits immediately the vision of stress singularities and analyses associated with the discipline of fracture mechanics. Nearly ten years ago, this thought initiated an analytical/numerical study of the stress field surrounding a step discontinuity in a composite (Kubr, 1990) in order to lay the groundwork for further experimental examinations. Treating each ply as a continuum with anisotropic properties and the corner as a mathematically sharp 90° feature as the origin of a (polar) coordinate system, it was found that the stresses were of the form $\sigma_{ij} = \Psi_{ij} r^k$ and thus similar to the Williams solution for a wedge in an isotropic material (Williams, 1957). The use of a highly refined finite element mesh rendered the values of k and Ψ by using plots of $\log(\sigma)$-$\log(r)$ for each stress component, a procedure followed also recently by Zenkert et al. (1997). This solution was valid, however, only for distances of less than 10^{-1} μm from the corner. Considering that the diameter of an individual fiber is about 5–7 μm, the power law is valid in such an extremely small region that continuum concepts for "smeared-out" ply properties are not applicable. Consequently, one must call the treatment of failure from a corner in a composite lay-up by means of singularity analyses into question.

A subsequent, and corollary, microscope study (Gortsema, 1992) further supported this conclusion in that it demonstrated that failure initiation consistently emanated not from the corner, but typically occurred at some distance, measured in terms of ply-thickness, away from that location. One reason was that the corner was not "analytically" sharp, regardless of how carefully the specimen preparation was carried out. The implication of this finding for structural analysis is clearly that micromechanical considerations should not be expected to dominate structural failure analysis in this context, and that macroscopic failure proclivity must be evaluated at an appropriate size scale. Moreover, from a design point of view it is desirable to evaluate structures in terms of "strength of materials" loads such as moments, (average) shear and tension stresses. At issue is thus whether a failure criterion can be established that lends itself to structural applications. Even if the basis of such a criterion rests ultimately in the mechanics at the micron or submicron scale, it may be possible to identify a structural or "macroscopic" criterion or criteria, such that subsequently a minimum of test data suffices to establish a design guide.

Previous examinations of this and related problems have been addressed by others primarily by analytical/computational means. Based on generalizations of linearly elastic fracture mechanics these studies assume that the onset of fracture has been predicted in terms of a fracture toughness parameter. Stress singularities and approximate stress distribution around a (mathematically) sharp corner were obtained analytically by Lin and Hartman (1989) who used Lekhnitski's complex variables formulation, and by Kassapoglou and DiNicola (1992) who, like Bhat and Lagace (1994), provided simplified, design oriented stress estimations. Concerned with the failure of imperfect butt joints Zenkert et al. (1997) approached the analysis numerically, while experimental work by Hyer et al. (1990) and by Botting et al. (1996) emphasized the three dimensional nature of the stresses near sharp corners in ply drop-off configurations. Like the earlier study in our laboratory these investigations focused on the effects of singularities or stress concentrations at very small size scales.

Experimental studies have been typically conducted at environmental (room) temperatures. However, with the prospect of high speed air-transports and associated elevated temperatures in both primary load carrying as well as engine-close structures, the possible degradation of structural performance due

to raised temperatures must be considered. This is especially true for polymer matrix materials which become very temperature sensitive as their glass transition temperature is approached. It is thus important to evaluate in which temperature range below the glass transition structural penalties become severe. This temperature sensitivity manifests itself primarily in terms of increased time dependent (creep) behavior, which, even at temperatures well below the glass transition (20–30°C) may give rise to accumulated effects if repeated thermal cycles are involved. Although we recognize the importance of the time dependent behavior in the failure process of composite materials we prefer to take here a somewhat simpler point of view and consider temperature merely as a parameter which affects the failure strength of the composite potentially without a major complication in the form of time dependent (creep) response of the matrix. However, it is then still of interest to ask whether the failure mode(s) or mechanism(s) of failure initiation (and progression) is changed by elevating the temperature.

It appears self-evident that the ply sequence across the "interface" between the step-up and the base plays a significant role in the failure initiation process. For definition purposes we refer to the thicker portion in Fig. 1 as the step-up or stiffener, while the thinner portion is called the plate or skin, the two portions being separated by the "interface". From a physical point of view the "interface" is formed by co-curing and as such does not represent a manufacturing interface in the sense of a "secondary" or adhesive bond. The term is used here only for spatial identification purposes. Because the layers adjacent to this interface can control the failure behavior it was appropriate to include in this study several lay-ups that are likely to be representative of a large range of possible lay-up configurations, a number of four being deemed sufficiently indicative.

The tenor of this study is primarily experimental in nature, with, however a strong component of numerical analysis to examine an analytical basis for the observed failure behavior. It is not our primary objective to present design data, but to examine the nature of the interaction between loads defined in structural mechanics parlance and to explore to what extent these interactions can be explained in terms of known failure initiation concepts, most of which are well understood in the composites community. From a hardware design point of view it is important to know whether an interaction relation is complicated or not; for, if such a relation should turn out to be linear, even in the presence of nonlinearities induced by large deformations, then a minimum number of tests are needed for design purposes to establish engineering data in a particular application, while a more complicated relationship may entail costly testing every time such information is required.

Because the details of the experimental apparatus and the basics of the numerical analysis have been described elsewhere (Lee and Knauss, 1998), it suffices to present here only a brief account to the extent that it is necessary to understand the full presentation and implications of this study. Accordingly we summarize in the next section the specimen geometry and lay-up. The experimental arrangements are described in Section 3, including identification methods of failure initiation. Failure observations are recorded in Section 4. Although the emphasis is here on failure initiation we also track the residual strength of the specimens once failure initiation has occurred to final destruction. In Section 5, this exposition is followed by a presentation and discussion of the experimental results in terms of two

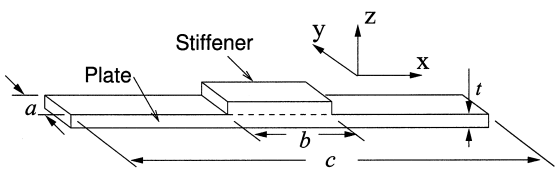

Fig. 1. Specimen configuration (c = 22.9 cm for loading device in Figure 2, c = 8.9 cm for loading device in Figure 3, b = 3.8 cm, t = 2 mm (0.08 in), a = 2.5 cm).

Table 1
Stacking orders of the specimens

Type	Plate	Stiffener
I	$[90,+45,0,-45]_s$	$[0,-45,90,+45]_s$
II	$[90,-45,0,+45]_s$	$[90,+45,0,-45]_s$
III	$[-45,90,+45,0]_s$	$[+45,90,-45,0]_s$
IV	$[0,-45,90,+45]_s$	$[0,+45,90,-45]_s$

failure criteria. While such a consideration cannot be exhaustive in a paper of this length, the attempt is made to facilitate understanding as well as raising questions or incentive for further definitive analysis. Section 6 delineates an examination of the failure initiation at elevated temperatures and the paper concludes in Section 7 with a summary overview.

2. Specimens

The specimen geometry used in this study is shown in Fig. 1. The specimens are made of AS4/3502 carbon fiber reinforced epoxy[1]. Details of the manufacturing process and ply properties are given in the Appendix A. All of the specimens were fabricated as a single, stepped plate, which was then cut into strips after the curing/cooling cycle was completed. Each of the cut specimens was C-scanned to ensure that no delaminations nor inclusions were present.

Although in applications thickness discontinuities tend to be long, as commensurate with the edge of a stringer, there was no simple or effective geometry that could have avoided the three dimensional stress field near the edges at the step in this configuration. The consequence of this needs to be reflected in the (finite element) analysis later on [see also (Lee and Knauss, 1998)]. Also, as a result of the strip character of the specimens the tensile and bending loads generate twist deformations, which are not prominently present or absent in applications. This fact is simulated here only to the extent that such twist is minimized through appropriately constraining the ends of the specimens during loading.

Four types of specimens with different stacking order were studied. The four lay-ups, each one identified as a "Type" with a roman numeral, are described in Table 1. The fiber direction of 0° is parallel to the "1-" or x-axis and positive fiber angles are measured from this axis in the counter-clockwise direction. For ready visualization of the interface arrangement these are also depicted in Fig. 5 without recording all of the laminae far from the interface.

3. Experimental arrangements

Having discussed the specimen geometry we turn next to describing their loading arrangements, as well as the means for detecting initial failures.

3.1. Loading devices

Two devices were designed to apply combined loads to the specimens. These have been described in

[1] The specimens were manufactured at NASA Langley research center; we are grateful to Dr. James H. Starnes and Mr. Allen Waters for supplying and machining the specimens.

detail elsewhere (Lee and Knauss, 1998) and are only summarized here. One of these devices, shown in Fig. 2, employed the tension/torsion modes of an MTS testing machine to provide tension and bending by converting the twisting motion through linkages into lateral loads so as to impose bending and tension loads in arbitrary sequence (non-proportional loading). The accompanying lateral force was recorded with a compression load cell. Because of the non-uniform cross section unidirectional tension produces also bending (Lee and Knauss, 1998). Loading with this device was accomplished typically by first imposing tension, and then adding the bending. This device allowed three- as well as four-point bending. Because early test results with this apparatus evidenced no significant differences under three- *vis-à-vis* four-point bending, it was concluded that transverse shear was not of primary importance in the failure process and was, therefore, not further included in our studies.

A second device, shown in Fig. 3, provided tension and bending in proportional loading through mounting the specimen eccentrically and subjecting the grips to tension only. The range of the eccentricity "e" varied from -2.5 mm (-0.1 in.) to 13 mm (0.5 in.). By adjusting the off-set, a range of bending/tension combinations is achieved, including zero bending, to counteract the effect of the "discontinuity in the neutral axis" at the step. The operation of this appliance was much simpler than the previous one, and was used primarily. As the results derived from either loading device did not differ within the range of data scatter, the loading path was judged to be unimportant in this study.

Because the deformations were classified as "large", being on the order or larger than the specimen thickness, the bending moment needed to include the deformations. This was accomplished by measuring the distance, w, between the line of tension (centerline of the MTS grips) and the mid plane

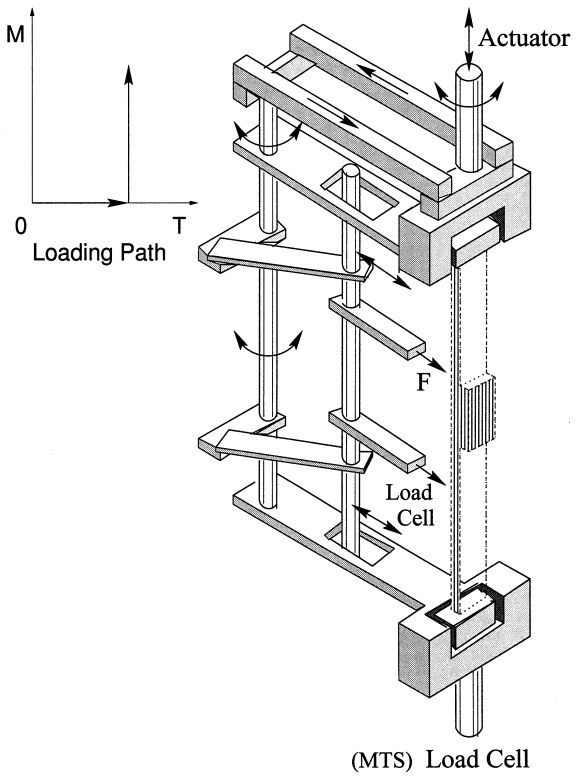

Fig. 2. Loading frame for three- and four-point bending coupled with tension.

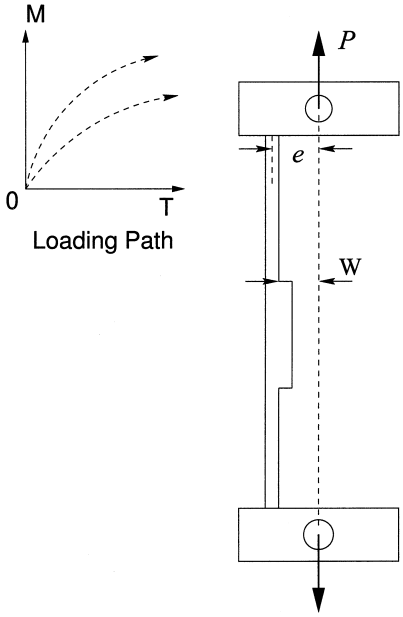

Fig. 3. Loading frame for proportional moment-tension loading.

of the step section in the deformed configuration. Since the error in this moment determination is directly proportional to the error in the measurement of the displacement "w", it was imperative to make this measurement with maximal precision. This was accomplished with a low power (monocular) traversing microscope [see Fig. 4 for the set-up] allowing a resolution of 0.025 mm (0.001 inches); this method avoided contact forces lateral to the specimen and could be employed at elevated temperatures.

3.2. Observation of failures

At room temperature observations of failure initiation were made with the aid of a second (stereo) microscope while the specimen was under load. The stereo microscope was placed on a mount possessing three degrees of freedom that allowed following the region of interest undergoing deformation as first cracks appeared. According to the numerical stress analysis (Lee and Knauss, 1998), the region of highest stresses was well identified for Type I and II specimens so that the location of the failures was reasonably well identified at the edge of the specimens after a few trials. Attachment of an optical camera to the microscope and a polished surface finish on the specimen edge allowed thus the recording of the various features in the damage development during the (room temperature) tests. Accompanying the optical record, the cracking produced an audible energy release, a feature that became important in situations where failure initiation was difficult to observe on the specimen edge directly, as, for example, at elevated temperatures or with specimens of Type III. In the latter, the top lamina of the plate had the fibers running at 45° with respect to the tension axis and initial cracking did not always occur near the specimen edge but along the corner or edge of the step across the specimen. In these situations the crack-induced audio signal noted the failure. At this point the test was stopped, the specimen was removed from the test frame, and the surface examined for cracks with the microscope and with a dye-penetrant. For tests at elevated temperatures the audible signal was used exclusively for failure indications. Failure observations required relatively large magnification, but because of the multiple glass panes of the temperature control chamber this mode of observation became difficult. On

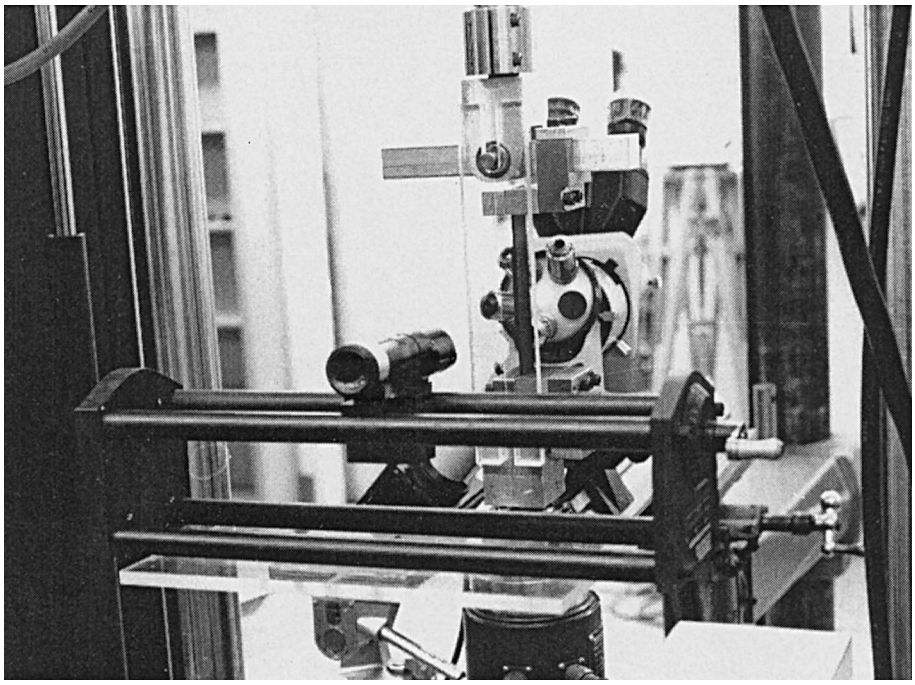

Fig. 4. Traveling microscope for measuring lateral deflection.

the other hand, the low-power observation of the deformation through the traveling microscope was still feasible.

4. Failure behavior

The failure behavior depended clearly on the stacking sequence, differentiated here primarily in terms of the ply orientation next to the interface. We delineate the major differences between these sequences and examine the commonality in their failure behavior based on accepted criteria in the fiber composites community. The experimental results are discussed first[2], followed by analytical evaluations in the next section. A summary of the failure patterns associated with the four stacking sequences is sketched in Fig. 5: Although not all laminae are shown with clarity of presentation in mind, the ply orientation near the interface is properly identified.

4.1. Type I and Type II specimens

The failure response of these specimens is governed by the similarity in the specimens: For both types the stacking sequence of the plate are the same, though the stiffeners possess different ones, namely $[0,-45,90,+45]_s$ for Type I and $[90,-45,0,+45]_s$ for Type II, so that the stiffener lamina next to the interface has either a 0° or a 90° orientation. As sketched in Fig. 5, cracking occurred in the top ply of the plate where the (maximum) tension acted across the fibers. The interaction between moment and

[2] The relative paucity of data results from a limited supply of specimens and was not a matter of convenience.

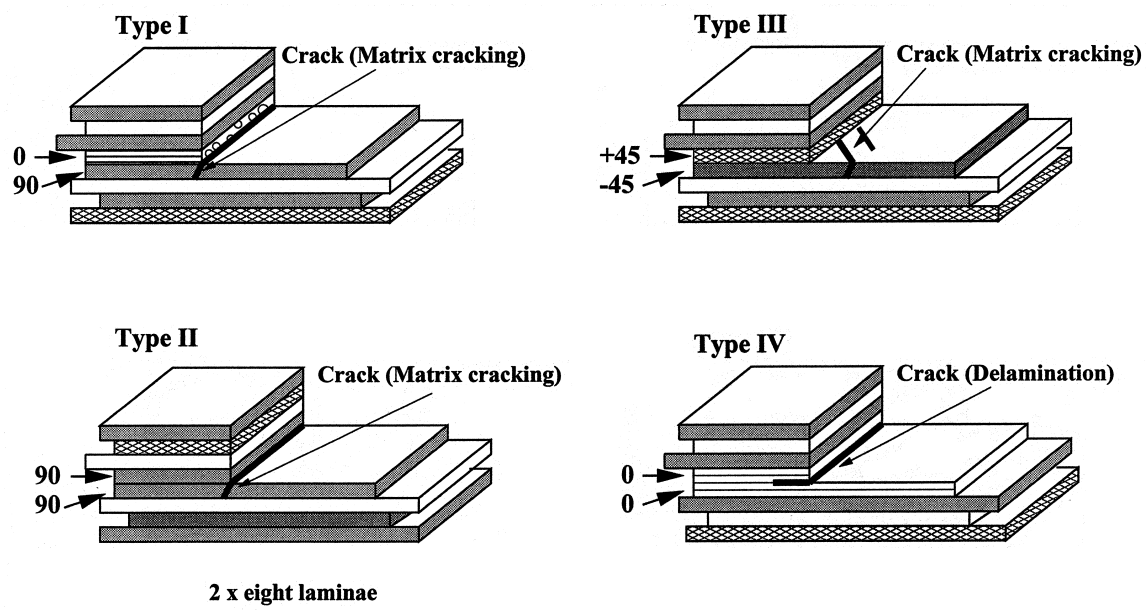

Fig. 5. Failure modes.

tension at failure initiation for the two lay-ups are presented in Fig. 6. Disregarding for the moment the analytically developed lines, we note that in spite of the large deformations, the interaction between moment and tension at failure is roughly linear[3], and that the load levels for the Type II specimen are typically higher by about 25% than those for the Type I specimens.

The question arises in this connection whether the assertion that failure occurs at distances away from the corner is merely an artifact of the observation method and whether failure was indeed precipitated by a singularity stress field, which, however was not observed on the edge of the specimen. To examine that possibility the microscopic inspection was extended to the line along the step base across the specimen which procedure rendered the same results. In all these tests the correlation between the first appearance of a small crack and a distinctly audible sound was very close. When microscopic observation was difficult or not possible, this observation justified reliance in subsequent tests on (first) audible sound emission as the indicator of failure initiation.

Although the emphasis in this study is the initiation of failure, an effort was made to assess the remaining load carrying ability of the specimens. It was found that total failure resulted for these specimens at moment and tension levels that were about 25 to 35% percent higher than those at failure initiation.

4.2. Type III specimens

The layers across the interface in this specimen are oriented in the $\pm 45^{\circ}$ directions, resulting in crack formation in the top lamina of the plate and parallel to the fibers (tension across the fiber axes). Because the crack formation did not always start at the specimen edge it was also not always possible to identify initial failure through microscope observation. In these latter cases the sound was used to identify

[3] The question of a linear interaction will be discussed in more detail in the analysis section.

failure onset: On first hearing the characteristic noise, the test was stopped and the surface examined for cracks with the microscope and with a dye-penetrant. A picture of the latter situation is reproduced in Fig. 7, and the failure interaction data is presented in Fig. 8. Moreover, as for the previous types of specimens, complete specimen failure occurred again at about 25 to 35% higher values than those that initiated failure.

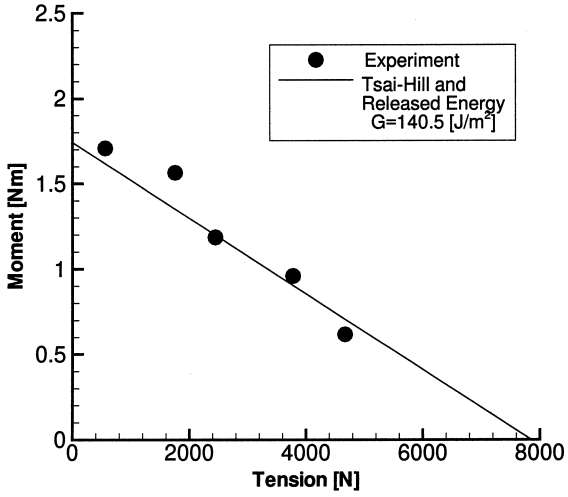

(a) Type I

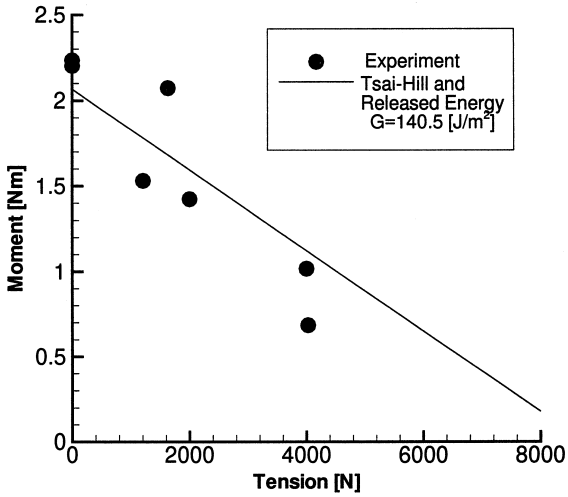

(b) Type II

Fig. 6. Moment-tension interaction for failure initiation in Type I and II specimens.

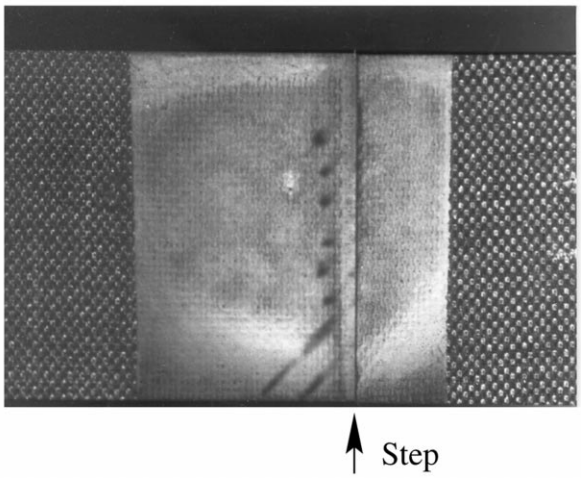

Fig. 7. Cracks in Type III specimens; thick strap section is to the right.

4.3. Type IV specimens

In this type of specimen the laminae adjacent to the interface possess only 0° orientations so that cracking across the plate lamina is not favored. Correspondingly, the failure occurs by delamination and subsequent fracture propagation and the failure initiation was different. The failure progressed in a narrow region parallel to the "interface", so that the resulting fracture surface was not smooth. It is also noteworthy at this point that the values of moments and tension at which failure is initiated, are higher by a factor of about two compared to those for the Type I, II and III specimens, where cross-ply fracture governed. Moreover, and in further contrast with the previous types of lay-ups, total failure followed the initiation process rather closely, so that load increases of only about 10% separated failure initiation and final loss of integrity. An edge view of the failure initiation is illustrated in Fig. 9, after which the delamination crack propagated further and opened as shown in the Fig. 10. Compared to the other types of specimens, the damage propagation was rather catastrophic as much of the stiffener separated from the plate. The interaction data between moment and tension at failure initiation are presented in Fig. 11.

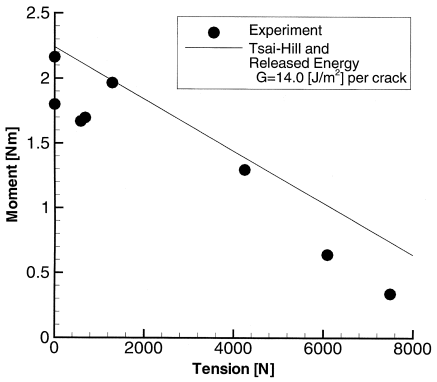

Fig. 8. Moment-tension interaction for failure initiation in Type III specimens

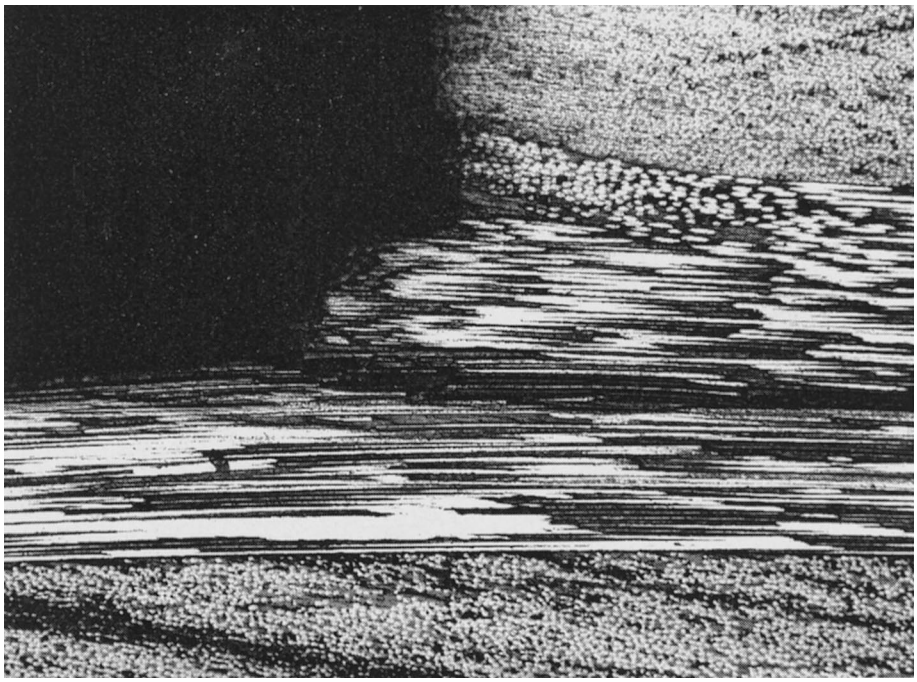

Fig. 9. Delamination initiation in a Type IV specimen.

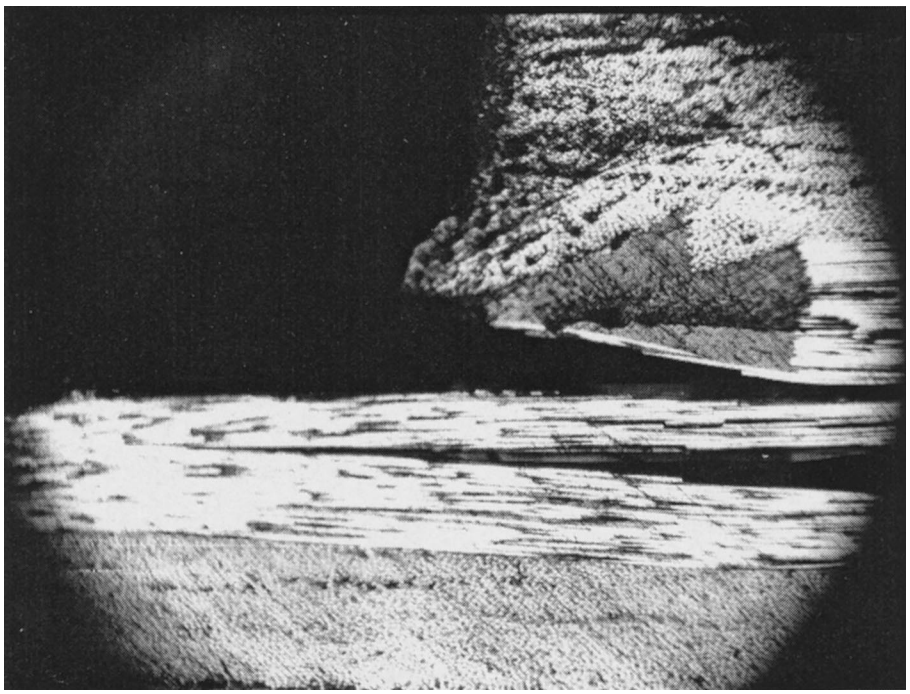

Fig. 10. Delamination and bridging in a Type IV specimen.

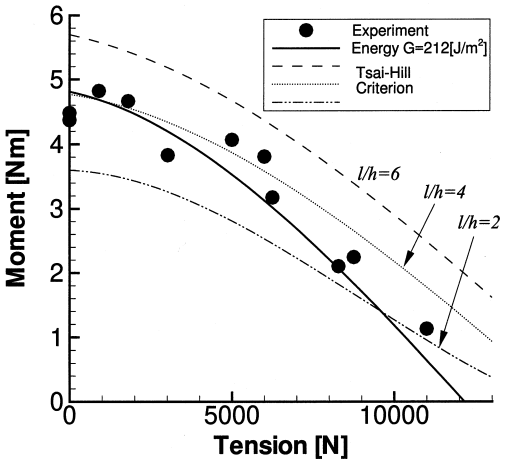

Fig. 11. Moment-tension interaction for failure initiation in Type IV specimens(l; crack length, h; the ply thickness)..

5. Analysis

We take recourse to finite element analysis for examining the conditions prevailing at failure initiation. Generally, two types of criteria offer themselves in this context, namely stress or strain criteria, as well as energy based measures. As an example of the former kind, the Tsai-Hill criterion is investigated here as being possibly adequate, while a "discretized" fracture energy criterion is suggested for the latter. To inquire whether a common criterion exists for the failure initiation process in all specimens, we pursue both criteria for all test situations; however, it will be found that no single set of material failure parameters for either type of failure characterization describes the data unequivocally, though broad rules for analysis can be outlined. While there are alternate rationales for failure analysis, it is beyond the scope of the current presentation to explore more criteria, leaving some of the remaining questions for future resolution.

The specimen, along with the end fixtures, are discretized for purposes of a finite element analysis as illustrated in Fig. 12, with the region of direct interest being then represented by a submodel as shown in Fig. 13. These computations, carried out with the aid of the ABAQUS code, are discussed in more detail in reference Lee and Knauss (1998).

In the context of failure analysis, the discretization scale for finite element computations deserves further discussion. We certainly recognize that any discretization may be called into question, because a finite element size makes sense ultimately only if it is scaled to a fillet radius or some other pertinent (smaller) dimension. It will be appreciated, however, that such detailed information varies too much from case to case to be a practical avenue for addressing failure initiation from thickness discontinuities. One thus has the choice of either postulating a "generic" or "typical fillet" radius or demand that each situation be analyzed according to a measured value. The latter proposition is clearly not practical, especially not for design purposes, since such "fillets" are neither well defined nor repeatable. Suggesting a generic radius is, however, tantamount to specifying a minimum discretization scale. We follow this latter avenue and choose a discretization scale that makes the test results consistent with the ultimate properties determined in separate tests (see the Appendix A). This approach required that the smallest (brick) element be chosen with its longitudinal dimension (= in the 1-direction in Fig. 13) equal to six times the ply thickness. For Type IV specimens the effect of this variation can be significant if a stress criterion is used, as will be demonstrated later on. Moreover, the element size effect will be considered in

more detail in connection with the energy based criterion. We reserve consideration of the analytical agreement or disagreement with the experimental results until all situations have been considered.

It suffices to point out here that the analysis was fully three-dimensional, each lamina being represented by a homogeneous, anisotropic medium; use of the ABAQUS code typically involved over 13,000 degrees of freedom for the base problem on a Cray 90. As developed in Lee and Knauss (1998) a sharp corner was avoided in the analysis through choosing the element size in the corner vicinity appropriately large.

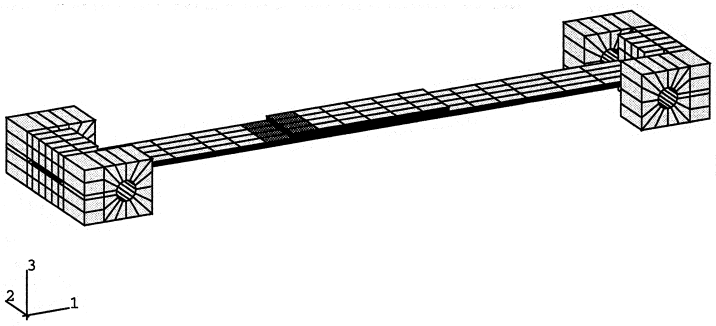

(a) Three- and four-point bending

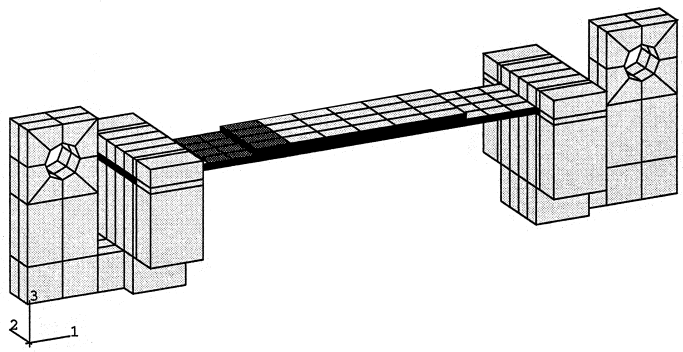

(b) Mesh for proportional loading

Fig. 12. Coarse finite element meshes for the two loading devices (the dark areas are domains for submodeling). (a) Three- and four-point bending. (b) Mesh for proportional loading..

5.1. Tsai-Hill failure criterion

Rather than develop new failure criteria it is our purpose to examine the degree to which existing criteria can be applied to a complex problem. A near-classical criterion for composite failure is the Tsai-Hill criterion, which includes the maximum stress or strain criteria as special cases. We examine the failure initiation for the four types of specimens from this point of view as one alternate or possibly more meaningful choice for failure analysis. The critical values for AS4/3502 are identified in the Appendix A as σ_{iu}, τ_{iju} in terms of which the Tsai–Hill equation is given (in terms of stresses) by

$$\left(\frac{\sigma_1}{\sigma_{1u}}\right)^2+\left(\frac{\sigma_2}{\sigma_{2u}}\right)^2-\frac{\sigma_1\sigma_2}{\sigma_{iu}^2}+\left(\frac{\tau_{12}}{\tau_{12u}}\right)\geq 1 \tag{1}$$

By this relation failure is imminent when the stress combination at any point in the specimen reaches or exceeds condition (1).

5.1.1. Type I and II specimens

For 90° fiber orientation the Tsai–Hill criterion reverts to that of a critical fiber-normal stress (or strain) once one recognizes that σ_{1u} is large compared to any other stress component, and that τ_{12} is (very close to) zero for the present case. One thus looks for the combination of tension and bending on the specimen such that, say, the normal stress across the 90° fiber direction reaches the critical value σ_{2u} = 57.6 MPa (see Appendix A), subject to the choice of the finite element size discussed above. The stresses and strains in the vicinity of the thickness discontinuity were determined, and the maximal normal stress (strain) orthogonal to the fiber direction was compared to the critical values. This includes the slight stress raiser in the corner of the specimen [see Fig. 13 in Lee and Knauss (1998)]. The comparison with the experimental data is shown in Fig. 6.

5.1.2. Type III specimens

For these specimens the full Tsai–Hill Eq. (1) applies because the fiber orientation across the interface induces shear stresses along the fibers. The computations are compared with the experimental data in Fig. 8, using the ultimate properties listed in the Appendix A, which were also used for the specimens of Type I and II above.

5.1.3. Type IV specimens

In applying the same kind of analysis to this specimen type one evaluates the criterion (1) "at the discontinuity". It became clear rather early in the analysis effort that the failure description of this specimen type was more susceptible to the choice of the finite element dimension near the step than the

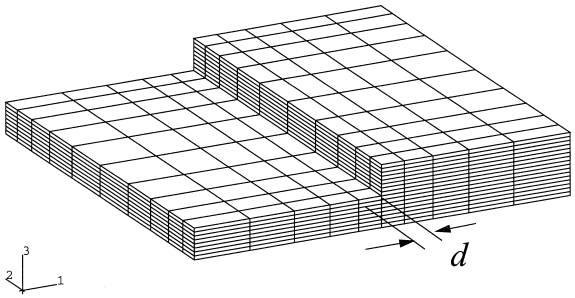

Fig. 13. Submodel of the step area. "*d*" denotes the smallest finite element dimension.

other specimens. Accordingly, we show in Fig. 11 the curves for three values of the element size. For comparison with the results in the next section, note that these relatively small changes in the element size occasion sizable variations in the loading at failure initiation.

5.2. Energy release rate computations

The concept of the energy release rate arises typically in fracture mechanics problems where it is associated with the propagation of a pre-existing crack by an arbitrarily small (infinitesimal) growth step. In the present study the initial geometries are all considered to be crack-free, so that, strictly speaking, energy release rates are not defined. However, we apply this concept to situations where a small but finite crack length is generated from an initially (and apparently) crack free geometry, and refer to this discrete process as the (discretized) energy release rate procedure.

The method for determining the energy release rate G was similar to the finite element formulation of a crack closure integral technique employed by Rybicki et al. (1977). Essentially the same discretization is used for the crack-free geometry to evaluate the deformations and stress states in the sample along with its supports that was used for the computations involved in evaluating the Tsai–Hill criterion. Deviations from this practice will be discussed as they arise. Two submodels, one with and one without a crack (*cf.* Fig. 13) were analyzed (using the same boundary conditions) and the difference between the total strain energies of the two models was determined to represent the energy release rate G.

One question that arises again naturally concerns the length of the crack generated under these circumstances. In the case of trans-laminar fracture the crack typically appears "suddenly" across the whole thickness of the lamina. It is thus natural to accept the lamina thickness as the prevalent crack extension dimension. On the other hand, when the crack propagates parallel to laminae and parallel to the fibers as demonstrated later for specimens of the Type IV, the crack extension distance for analytical purposes is not predetermined. For this reason, a parametric study has been included that varies the crack extension distance to assess the sensitivity of the method to variations in the initiated crack length: We ask then, what energy release rate is required to make the computations agree with the measurements. Thus, subsequently determined energy values are the result of optimally fitting the analysis to the experimental data.

5.2.1. Type I and II specimens

Fig. 14 demonstrates the appearance of a crack (model) at the base of the step. The computations

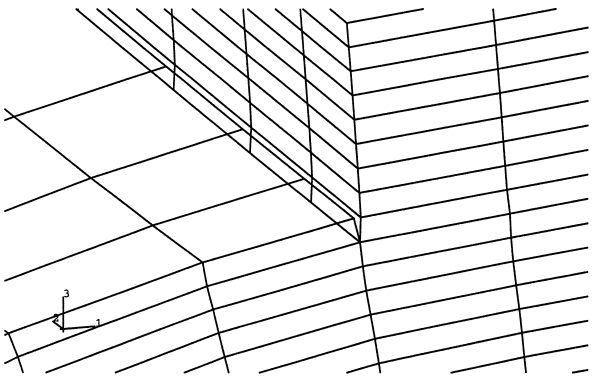

Fig. 14. Submodel detail of a crack for Type I and II specimens.

(can be made to) agree with the experimental data in Fig. 6(a) (Type I) and Fig. 6(b) (Type II) if the fracture energy is taken as 140.5 J/m^2 (0.8 lb/in.).

5.2.2. Type III specimens

It was observed, as shown in Fig. 7, that multiple cracking of the plate or skin occurred along 45° cracks that typically emanated from the step but did not extend across the specimen width. The number of cracks varied, as did their length. This fact may make a rational application of an energy release rate criterion in this situation equivocal, at least without further detailed studies, since the number of cracks per unit length of step is not clearly defined *a priori*. Certainly, the appearance of multiple cracks along the edge of the step discontinuity changes the release of energy in the structure in a discrete way so that a determination of energy consumption per unit of crack surface cannot be defined except for a single crack.

For completeness of presentation, however, the energy release rate for a single crack parallel to the fibers was computed for various lengths. After the length reached a value of ten or more times the ply thickness, the energy release rate was not materially affected. The comparison between computations and experiment is shown in Fig. 8 on the basis of a single crack per specimen which consumes energy at the rate of 14 J/m^2. This single-crack-value is clearly and significantly lower than that found for specimen Types I and II.

5.2.3. Type IV specimens

Having already discussed briefly the question of what the effect of different initial crack lengths is on the application of an energy release rate approach (see also further below on this point), an additional concern arises with respect to the role of shear along the fracture path (multi-mode fracture). Recall for clarification that while we have referred to an "interface" between laminae adjacent to the step, this is not an interface in a physical sense; specifically, for specimens of Type IV that "interface" is really in the center of the two identically oriented laminae that belong, one each, to the plate and to the stringer, respectively. Nevertheless, one may ask whether the complex stress distribution, involving shear and normal stresses, impacts the failure behavior through mechanisms related to interfacial failure progression. Because there exists no stress singularity, the standard description of a mode mixity in terms of stress intensities is not appropriate and we use, instead, stress ratios from the high strain region at the base of the step. This ratio gives an analogue mixity of 30–50°. If one compares that value with data from mode mixity experiments (Liechti and Chai, 1992) one finds that this ratio falls well within the (flat) region where the fracture energy is insensitive to mode mixity effects. We thus conclude that mode mixity considerations do not play a role in this failure behavior.

Fig. 11 shows the comparison of experimental results with the computations for an energy release rate of 212 J/m^2 which is, if not identical, though on the same order as the value reported by Whitney et al. (1982) for an interlaminar fracture energy of 161 J/m^2 (0.92 lb/in.) of AS4/3502. The potential effect of different fracture step sizes on the energy release rate has been examined as shown in Fig. 15 where the energy release rate is computed for different crack initiation lengths, with the average representing the value of 212 J/m^2. It is clear that the variation is modest and is, in fact, considerably smaller than the experimental data scatter.

To summarize the examination of the energy release rate as a criterion for fracture initiation in this problem one finds that

(a) the general shape of the tension-moment interaction curves are well represented through this criterion for all types of specimens studied; on the other hand
(b) the value of the energy release rate that brings experiment and analysis into coincidence appears

to be a function of the stacking sequence, at least at the size scale of comparison underlying the present study:

To examine whether closer agreement can be achieved (same energy values for all specimens) if the analysis is carried to the size level of the fibers was considered to be beyond the scope of the study, and needs to be investigated separately. So much seems clear, however, that the significantly higher value of the energy level for the Type IV specimens is, most likely, the result of multiple fractures at different levels through the thickness of the two adjacent zero-orientation layers; this is the same arrangement that leads to fiber bridging in a continuing intralaminar fracture or delamination process.

5.3. Discussion

Let us examine the consistency of both failure criteria to "explain" failure initiation and whether one or the other criterion provides a "better" estimate. To start with, we note that either criterion provides for an essentially linear interaction between tension and bending for Types I, II and III, but a roughly parabolic characteristic for those of Type IV. For specimen Types I–III (Fig. 6(a), Fig. 6(b), Fig. 8) only one numerical-analytical trace is shown for both the Tsai–Hill or the energy criterion: Within computational resolution there was no distinction. The other reason for this "coincidence" was that the energy release rate G was adjusted to render the same trace, but the energy criterion and the Tsai–Hill criterion provided the same slope. With respect to Fig. 11 one may argue that the energy criterion provides a somewhat better representation of the experimental data than the Tsai–Hill criterion. What makes that proposition somewhat more attractive is the fact that a single fracture energy renders this result with a relative insensitivity to the size of the finite element discretization and/or the postulated crack length. By implication this result indicates that the issue of fillet radius or finite element size scale is minimized if an energy approach is taken for a lay-up exemplified by the Type IV specimens.

Although the functional representation of the failure data by the energy criterion appears to be good, one must question this uniformity in terms of the single-valuedness of the energy release rate parameter. Type I and II specimens should involve essentially the same parameter by virtue of the fact that the lay-

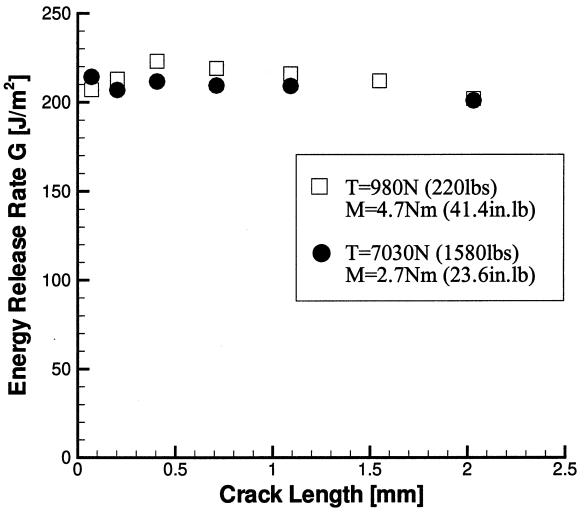

Fig. 15. Sensitivity of the discretized energy release rate to the size of the released crack surface in Type IV specimen for two loading conditions ($h = 0.25$ mm).

up is very similar. Apart from this similarity, there are then three groups of specimens which involve significantly different energy parameters: Specimens I and II yield 140.5 J/m^2, Type IV requires 212.0 J/m^2, and Type III specimens are consistent with a value of 14.0 J/m^2. Clearly, this "problem" invites further attention.

On the other hand, the Tsai–Hill criterion produces a correlation with the test data through a single set of material parameters (see Appendix A), which, however, does not replicate the shape of the interaction curve very well for the type IV specimens. Moreover, it makes that analysis particularly sensitive to the finite element discretization. Clearly, there is, again, room for improvement of the theoretical explanation for this behavior.

Recall that a strong motivation for this work was the need for developing design-oriented guidelines. From that point of view a combination of criteria may be the most prudent answer to this dichotomy: When the stacking sequence favors transverse ply-fracture the simplest way to estimate failure initiation is to employ a stress or strain criterion; when delamination or intra-ply separation occurs, an energy based criterion provides adequate strength estimates.

Perhaps the more important conclusion for the design process is, so far, the general character of the curves for different stacking sequences. This understanding allows the engineer to perform a minimum number of tests which may provide sufficient information to fix the parameters for the design process, based on one or the other model. According to the suggestion in the previous paragraph, this would be a linear relation for cross-ply failure and a parabolic curve for a delamination type of failure. Also, as more data become available on the failure of thickness step geometries this concepts will be refined or firmed up further.

6. Effect of elevated temperature

In the previous section, the failure at thickness variations have been recorded and discussed for room temperature conditions. The same procedures were followed to investigate failures under elevated temperatures for several of the stacking sequences. The combined loading frame and specimens were placed in an environmental chamber to control the temperature. Two temperatures, 100°C and 150°C, were chosen, considering that the glass transition temperature of the matrix is 198°C.

Experimental procedures for high-temperature tests were the same as those at room temperature except for the failure detection method. It was, at least initially, desired to observe the failure initiation under magnification inside of a thermal control chamber in spite of intervening glass panes. This objective was pursued by constructing an optical set-up, essentially with the help of long-focal lenses (f = 30 cm), to form a virtual image of the specimen surface inside the temperature cabinet but external to it; the virtual image could then be examined and enlarged through microscope observation. However, with this optical arrangement it turned out that it was, practically speaking, too difficult to locate and track the corner of the specimen and to focus on it through the multiple glass panes of the chamber so as to follow failure that might contain a creep or time-related effect. Instead of this microscope method, the acoustic emission method was, therefore, used to detect the initiation of failure because the correlation between acoustic emission and crack appearance had been established in numerous previous tests at room temperature.

The finite element analysis accompanying the high temperature experiment accounted for both the mechanical loading as well as for temperature induced stresses, assuming the specimens to be stress-free at 25°C (see Appendix A). Changes in the mechanical properties with temperature were also taken into account. Because the modulus in the fiber direction is dominated by the fibers rather than by the matrix, that modulus remained unchanged. The property values at elevated temperatures were estimated from the available information according to the outline in Appendix A.

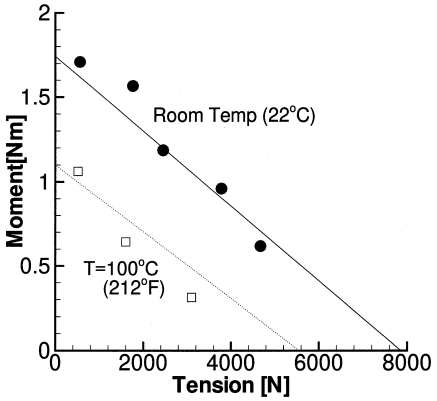

Fig. 16. Moment-tension interaction at failure initiation for Type I specimens at two temperatures.

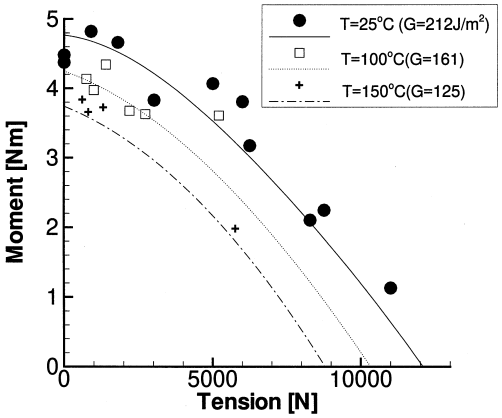

Fig. 17. Moment-tension interaction at failure initiation for Type IV specimens at three temperatures. Curves are based on energy release rate computations.

The test results and corresponding computations are delineated next. Because the modeling has been considered in some detail on the room temperature data, not all the computations were repeated for the data obtained at elevated temperatures. The specimens of Type I are analyzed in terms of the Tsai–Hill criterion only. No data could be acquired for the Type II or III specimens.

6.1.1. Type I

Testing specimens of Type I at 100°C exhibited identical failure characteristics to those at room temperature: The failure mode was again by transply matrix cracking. However, the magnitudes of the failure loads were lower than those at room temperature: Fig. 16 shows the comparison of the data with the numerical fit according to the Tsai–Hill criterion.

6.1.2. Type IV Specimens

Again, as for specimens of Type I, the failure loads at elevated temperatures for this specimen type were lower than those obtained at room temperature. However, the relative differences are now smaller

as may be deduced from Fig. 17. The finite element analysis for computing the failure loads was carried out now only on the basis of the energy release rate concept. The critical energy release rates at 100°C and 150°C are 161 and 125 J/m^2, respectively. This critical energy value dropped thus by about 0.7 J/m^2 per degree °C.

In this context it is of interest to discuss the potential effect of material properties variations on the energy release rate values. The individual ply properties other than those with zero orientation (in the tension direction) were varied in the computations by as much as 20%; the resulting change in the energy release rate was between only one and two percent, making the latter characteristic rather insensitive to stiffness variations other than those in the zero plies. Correspondingly one finds that if one were to allow the room temperature moduli to prevail uniformly at the elevated temperatures, one would find an energy release rate that is only 6% higher than that derived from the temperature degraded stiffnesses.

7. Conclusion

Experimentally determined failure initiation in laminated composites containing "sharp" corners has been presented for three temperatures (22, 100 and 150°C) along with numerical evaluations. Within experimental scatter, three-point and four-point bending yielded identical results. This indicates that transverse shear does not contribute materially to the failure response, thus leaving tension and bending as the major interactors for failure initiation. Bending moments have been included which enhance fracture; reversal of the moment sign presumably reduces fracture proclivity, but that variation has not been studied extensively. A few measurements have been acquired for either small or reversed bending moments so that primarily tension induced failure resulted. In these tests (at room temperature and $-1.1\ \text{Nm} < \text{Moment} < +1.1\ \text{Nm}$) the failure occurred typically at a constant tension stress of 207 MPa in Type IV specimens.

Depending on the stacking sequence next to the "interface" of the step either transverse ply cracking or delamination occurs. Specimen containing fiber orientations on either side of the "interface" and having an orientation component deviating (significantly) from the zero direction (specimen Types I, II, and III) fail by ply-fracture normal to the fiber orientation in the top ply of the plate. Subsequent failure progression occurs by ply delamination and additional ply fractures. On the other hand, when the interface between the steps is contained between two layers of zero-oriented fibers (specimen Type IV) a delamination-type failure results.

While the appearance of sharp corners invites analyses in terms of stress singularity (Kubr, 1990), this study shows (Gortsema, 1992) that fillet-like geometries resulting uncontrollably from any manufacturing processes call for evaluations employing non-singular stress field analysis. Accordingly, finite element computations relying on discretization with lamina thickness as the dimension governing element sizes appear quite adequate. To what extent this discretization applies to other composite materials needs to be investigated. With a view towards design related issues, it appears, however, that this type of analysis provides sufficiently accurate descriptions of the failure initiation process. Both stress (strain) criteria in terms of the Tsai–Hill criterion as well as a discretized energy release rate approach have been used to analyze the data.

In spite of kinematical nonlinearity in the experimental arrangement, the calculated interaction between moment and tension at failure is essentially linear (geometrically non-linear analysis) for the cases involving transverse ply failures. For these situations the Tsai–Hill criterion provides good overall correlation with a single set of material parameters, while the energy release computation provides an equally good fit to the data, but at the expense of a (non)common energy release. We note that even though it might be possible to obtain a closer "fit" of the (Tsai–Hill) computations to individual sets of

data for the separate lay-ups, we have refrained from doing so in the interest of applying a uniform criterion to all tests and configurations. Although the following observation is not perfect nor unequivocal, the delamination governed failure appears to be represented somewhat better by an energy criterion. This observation is consistent with the mode of failure progression and turns out to be rather insensitive to the size of the release increment. By contrast, the Tsai–Hill criterion requires a closer definition of an effective size scale (element size) near the step for Type IV specimens.

In the range studied, the effect of temperature on the failure manifests itself primarily in a lowering of the load levels, leaving the modes of failure unaltered. While at temperatures within a few degrees of the glass transition this behavior may change, particularly as the result of more time dependent material response, in the presently used environment higher temperatures primarily reduce the material strength. To describe a consistent failure behavior one must incorporate the thermally induced stresses in the overall evaluation, to the degree that the latter contribute a significant portion of the total and final stresses.

The specimens exhibiting the delamination mode of failure (Type IV specimens) provided the highest strength as measured by load carrying ability. They are nearly twice "as strong" as the other types of specimens which failed by ply fracture. However, the "stronger" configuration allowed for a markedly smaller (10%) difference between loads at failure initiation and final (total) failure than the ply-failure modes; the latter provided an additional load carrying capability of about 25 to 35% beyond that at failure initiation.

Acknowledgements

This work was supported by NASA Langley Research Center under NASA Grant NSG 1483. The authors would like to acknowledge the continued encouragement by Dr. J. Starnes and the assistance of Mr. Waters for providing the specimens. Substantial portions of the finite element computations were conducted on the Cray 90 at the NSF supported Supercomputing Center of the University of California at San Diego. We thank Dr. N. Pagano of the Air Force Materials Laboratory at the Wright Aeronautical Laboratories, for referring us to the data for AS4/3501-6.

Appendix A. Material information

The specimens were prepared by first forming the skin or plate from eight plies of prepreg material placed on a bleeder cloth that rested on an aluminum support plate. At this stage the pre-assembly was degassed (vacuum exposure) in the "wet" condition and a second panel with the lay-up appropriate for the stiffener was prepared, from which strips of the proper width were cut and similarly degassed, before being joined "wet" to the plate (skin). The three flat sections of this stepped assembly were covered with bleeder cloth, bagged and degassed before being placed in the autoclave. The cure profile followed essentially the recipe recommended by Hercules (Hexcel), except that 689 kPa (100 psi) were used instead of 586 kPa (85 psi). The temperature was ramped to 120°C in 60 minutes and then allowed to increase slowly to reach a steady state temperature of 135°C in two hours. After an additional 40 minutes, (time = 160 minutes) full pressure was applied and maintained continuously. From 205 to 225 minutes the temperature was raised to 177°C (350°F) and held for two hours thereafter, following which it was allowed to reach room temperature over a span of 90 minutes. After an additional two hours under these conditions the pressure was released.

The resulting panel was flat (did not curve away from the aluminum support plate), which was taken as a measure of no or very low residual stresses in the panel. The strip specimens were then cut from the

Table A1
Properties of dry AS4/3502

Property	22°C	100°C	150°C
E_{11}^{T} [GPa]	141.3	141.3	141.3
E_{22}^{T} [GPa]	11.5	8.5	7.4
G_{12} [GPa]	6.0	5.6	5.4
σ_{1u} [GPa]	1.4	1.4	1.4
σ_{2u} [MPa]	57.6	42.6	37.0
τ_{12u} [MPa]	120.0	112.0	108.0

Table A2
Properties of "wet" AS4/3502

Property	−55°C	71°C	121°C	130°C
E_{11}^{T} [GPa]	143.4	141.3	138.6*	143.6*
E_{22}^{T} [GPa]	11.7	9.3	8.2*	8.0*
G_{12} [GPa]	6.2	4.1	1.6*	
ν_{12}	0.35	0.30		0.28*
ϵ_{11u}	0.0087	0.0093		0.0098*
ϵ_{22u}	0.0048	0.0038		0.0034*
$2\epsilon_{12u}$	0.0199	0.0199		

panel with a diamond saw. The individual strip specimens were still flat as judged by observation with the unaided eye.

The following material parameters were used in the analysis. These data were acquired at Lockheed, Georgia and made available to us through NASA Langley. The parameters identified with an asterisk were taken from (U.S. Army Research Laboratory, 1994) (see Tables A1 and A2).

The properties at elevated temperatures were available only for "wet" conditions. To estimate appropriate properties for dry conditions the properties of a similar composite, namely AS4/3501-6, were studied. For this material, data for "dry" and "wet" conditions at −25, 24, 75 and 125°C were recorded by Crasto and Kim (1997). These data for AS4/3501-6 were normalized by the respective values at 24°C and the appropriate fractions were plotted against temperature and extrapolated to 150°C. These plots provided ratios between "dry" and "wet" property values, which ratios were then used to compute the "dry" value proportionately from the "wet" values for AS4/3502. These are the data entered in the table above. The value of the fiber dominated E_{11} was unaffected by the temperature or moisture, as is readily verified by the available data.

Compared to the modulus data the ultimate strain values did not change systematically as a function of temperature and were thus taken as constant where necessary or desired.

References

Bhat, N.V., Lagace, P.A., 1994. An analytical method for the evaluation of interlaminar stresses due to material discontinuities. Journal of Composite Materials 28 (3), 190–210.

Botting, A.D., Vizzini, A.J., Lee, S.W., 1996. Effect of ply-drop configuration on delamination strength of tapered composite structures. AIAA Journal 34 (8), 1650–1656.

Crasto, A.S., Kim, R.Y., 1997. Hygrothermal influence on the free-edge delamination of composites under compressive loading. In: Composite Materials; Fatigue and Fracture (sixth volume), ASTM STP 1285, pp. 381–393.

Gortsema, S.C., 1992. An Experimental Investigation of the Failure of a Stepped Composite Plate. Ae.E. Thesis, Caltech, Pasadena, CA.

Hyer, M.W., Loup, D.C., Starnes Jr, J.H., 1990. Stiffener/skin interactions in pressure-loaded composite panels. AIAA Journal 28 (3), 532–537.

Kassapoglou, C., DiNicola, A.J., 1992. Efficient stress solutions at skin stiffener interfaces of composite stiffened panels. AIAA Journal 30 (7), 1833–1839.

Kubr, T.J., 1990. Stresses Near a Change of Thickness in a Continuous-Fiber-Composite Plate. Ae.E. Thesis, Caltech, Pasadena, CA.

Lee, S., Knauss, W.G., 1998. Failure of laminated composites at thickness discontinuities — an experimental and analytical study. Applied Composite Materials Journal 5 (5), 273–287.

Liechti, K.M., Chai, Y.S., 1992. Asymmetric shielding in interfacial fracture under in-plane shear. Journal of Applied Mechanics 59, 295–304.

Lin, K.Y., Hartman, H.H., 1989. Numerical analysis of stress singularities at a bonded anisotropic wedge. Engineering Fracture Mechanics 32 (2), 211–224.

Rybicki, E.F., Schmueser, D.W., Fox, J., 1977. An energy release rate approach for stable crack growth in the free-edge delamination problem. Journal of Composite Materials 11, 470–487.

U.S. Army Research Laboratory, 1994. Department of Defense Handbook MIL-HDBK-17, Polymer Matrix Composites, vol. 2, Materials Properties, Materials Sciences Co., Fort Washington, PA.

Whitney, J.M., Browning, C.E., Hoogsteden, W., 1982. A double cantilever beam test for characterizing mode I delamination of composite materials. Journal of Reinforced Plastics and Composites 1, 297–313.

Williams, M.L., 1957. On the stress distribution at the base of a stationary crack. Journal of Applied Mechanics 24, 109–114.

Zenkert, D., Schubert, O., Burman, M., 1997. Fracture initiation in foam-core sandwich structures due to singular stresses at corners of flawed butt joints. Mechanics of Composite Materials and Structures 4, 1–21.